Talanta 118 (2014) 375–381

Contents lists available at ScienceDirect

Talanta

journal homepage: www.elsevier.com/locate/talanta

Miniaturised wireless smart tag for optical chemical analysis applications

Matthew D. Steinberg [a], Petar Kassal [b], Biserka Tkalčec [b], Ivana Murković Steinberg [b,*]

[a] GoSense Wireless Ltd., Moorfield Road, Duxford, Cambridge CB22 4PP, UK
[b] Faculty of Chemical Engineering & Technology, University of Zagreb, Marulićev trg 19, HR-10000 Zagreb, Croatia

ARTICLE INFO

Article history:
Received 24 July 2013
Received in revised form
7 October 2013
Accepted 15 October 2013
Available online 23 October 2013

Keywords:
Radio-frequency identification
Near field communication
Wireless sensor
Absorption spectroscopy
Photometer
Internet of things

ABSTRACT

A novel miniaturised photometer has been developed as an ultra-portable and mobile analytical chemical instrument. The low-cost photometer presents a paradigm shift in mobile chemical sensor instrumentation because it is built around a contactless smart card format. The photometer tag is based on the radio-frequency identification (RFID) smart card system, which provides short-range wireless data and power transfer between the photometer and a proximal reader, and which allows the reader to also energise the photometer by near field electromagnetic induction. RFID is set to become a key enabling technology of the Internet-of-Things (IoT), hence devices such as the photometer described here will enable numerous mobile, wearable and vanguard chemical sensing applications in the emerging connected world. In the work presented here, we demonstrate the characterisation of a low-power RFID wireless sensor tag with an LED/photodiode-based photometric input. The performance of the wireless photometer has been tested through two different model analytical applications. The first is photometry in solution, where colour intensity as a function of dye concentration was measured. The second is an ion-selective optode system in which potassium ion concentrations were determined by using previously well characterised bulk optode membranes. The analytical performance of the wireless photometer smart tag is clearly demonstrated by these optical absorption-based analytical experiments, with excellent data agreement to a reference laboratory instrument.

1. Introduction

The past decade has witnessed significant advances in chemical sensing modalities, not least of all where technology improvements have allowed miniaturisation of chemical sensors and closer integration with electronic instrumentation and wireless communication technologies. Proponents of the Internet of Things (IoT) predict that there will soon be a vast number of connected devices, including chemical sensors, able to monitor and sense their ambient environment and to share this data with the internet and cloud-based computing services. At a system level, wireless data transmission clearly offers benefits for certain chemical sensors in certain applications. The main advantages of wireless sensing, which arise from the elimination of extensive wiring, are improved mobility, unobtrusiveness, lower installation costs and higher nodal densities [1]. Wireless chemical sensors and biosensors are destined to have ever greater application in healthcare diagnostics, environmental monitoring, process monitoring, food quality monitoring and security [2].

To meet the growing demands for in situ monitoring of different chemical analytes in these diverse application areas there is a need for reliable, low-cost, low-power devices that are compatible with wireless communications systems. In the last few years there has been an upsurge in wireless chemical sensing devices due to the availability of ubiquitous wireless standards, including the global system for mobile communications (GSM), Bluetooth, ZigBee, WiFi, radio-frequency identification (RFID) and more recently near field communication (NFC). The general availability of wireless technologies based upon open standards has provided a technology push for wireless chemical sensors (WCSs) and chemical sensor networks (WCSNs). This phenomenon has been described in detail elsewhere in review articles [3] and in application specific reviews of the agri-food [4], chemical process monitoring [5] and homeland security [6] sectors.

RFID/NFC is an interesting short-range radio technology for integration with chemical sensors due to the ultra low-power consumption, low implementation costs and relative low-level complexity. The predictions are that RFID is set to become a key technology of the Internet of Things (IoT) [7].

Several RFID-based chemical sensors have therefore been developed, including RFID tags with integral gas sensors for monitoring

Abbreviations: RFID, radio-frequency identification; NFC, near field communication; WSN, wireless sensor network; IoT, internet of things.

* Corresponding author. Tel.: +385 01 4597 287; fax: +385 0 1 4829 064.
E-mail addresses: imurkov@fkit.hr, ivana.murkovic@fkit.hr (I. Murković Steinberg).

0039-9140/$ - see front matter © 2013 Elsevier B.V. All rights reserved.
http://dx.doi.org/10.1016/j.talanta.2013.10.033

food quality [8], with olfactory sensors (electronic noses) for integration with low-cost printed RFID tags [9,10], and for disinfection control in hospitals [11]. Potyrailo et al. have developed multi-analyte gas sensors from RFID tags for the detection of organic vapours [12] and also for use in food logistics [13].

Optical detection modalities can bring certain advantages over other methods of detection in chemical sensing systems. Optical sensors are generally non-destructive, easily miniaturised, not affected by electrical or magnetic interference, and are relatively inexpensive [14]. There have been significant advances made in the development of low-cost optical chemical sensors due to improvements in performance, availability and cost of optoelectronic components, especially light emitting diodes (LEDs) and photodiodes. Light emitting diodes were first used in optical sensors in the 1970s [15], and have been used abundantly since. This is mainly due to their relatively low power consumption (compared to laser or laser-diode light sources), low cost, small size, robustness, and their availability over a broad spectral range (from ultraviolet to near-infrared) which makes them appropriate for the determination of a wide range of analytes. LEDs have thus been implemented in a number of low-cost and portable analytical devices [16–18]. Recent examples include low-cost optical detectors for protein determination [19], the development of portable colorimeters based on multiple LEDs for the determination of interferents in blood serum [20] and concentrations of common food dyes in food products [21]. Systems using LEDs as both light sources and detectors have been constructed for the detection of gases [22], as well as glucose in human serum [23].

Due to the advances made in both wireless sensing and optosensing, wireless optical chemical sensors as hybrid devices have evolved. For instance, LED-based sensors incorporating pH sensitive dyes have been integrated with commercially available transmitters to form a wireless chemical sensor network [24]. A colourimetric assay comprising a pH sensing strip with a wireless video camera on board a low-cost robotic fish has been developed for environmental sensing applications [25]. There are also several examples of RFID-based optical chemical sensors the first of which was a planar optical detector for the determination of pH by sensitive dye immobilised in a thin sol-gel film [26]. More recently, Yazawa et al. at Hitachi Central Research Ltd have reported ultra-miniature optical RFID circuits for use in genetic analysis [27].

In order to address the growing need for integration of diverse chemical sensing techniques with RFID tag technology, we are developing an RFID sensor platform that is compatible with different types of (bio)chemical sensors – including optical, conductometric, potentiometric and amperometric (Fig. 1). Appropriate transduction mechanisms and interfaces for various sensor types are being implemented directly on the tags. So far, an RFID smart card for conductometric sensors [28], an RFID/NFC resistivity and temperature probe for monitoring the microenvironment in aggregate materials [29] and an RFID chemical sensor for measuring pH by optical absorption spectroscopy [26] have been developed. More recently, the RFID potentiometric measurement of pH was reported by us [30], and latterly a diverse range of cations relevant to *vanguard* monitoring [31] of water quality with solid-contact ion-selective electrodes were successfully measured with our RFID potentiometer [32].

In the work presented here, we demonstrate the characterisation of an ultra low-power RFID wireless sensor tag with an LED/photodiode-based photometric input.

The performance of the wireless photometer has been tested through two different model analytical applications. The first is photometry in solution, where colour intensity as a function of dye concentration was measured. The second is an ion-selective optode system in which potassium ion concentrations were determined by using bulk optode membranes.

2. Materials and methods

2.1. Experimental set-up for smart tag based photometry

The experimental set-up is shown in Fig. 2. The measuring system comprises the credit card sized radio-frequency smart tag, the sample cuvette with LED and photodiode (optical cell), RFID reader and a personal computer. The photometer is wirelessly linked to the personal computer through a commercial RFID reader (Ridel 5001, TAGnology GmbH, Graz, Austria) which energises and communicates with the photometer over a range of up to 10 cm.

2.1.1. Radio-frequency smart tag

The radio-frequency smart tag used here has been described in detail elsewhere [26]. In brief, the credit card-sized tag (Fig. 2) was developed around a commercial microcontroller (PIC12F683, Microchip Technology Inc., Chandler, AZ, USA) based on the ISO15693 RFID standard. Code for the microprocessor was written, developed and programmed into device's flash memory using an integrated development environment and device programmer (MPLAB v8.0 with PICStart plus, Microchip Technology Inc., Chandler, AZ, USA). The circuitry was designed using a schematic capture design and printed circuit board layout suite (EASY-PC Professional v11.0, Number One Systems Ltd., Gloucester, UK). Printed circuit boards were fabricated from standard FR4 materials

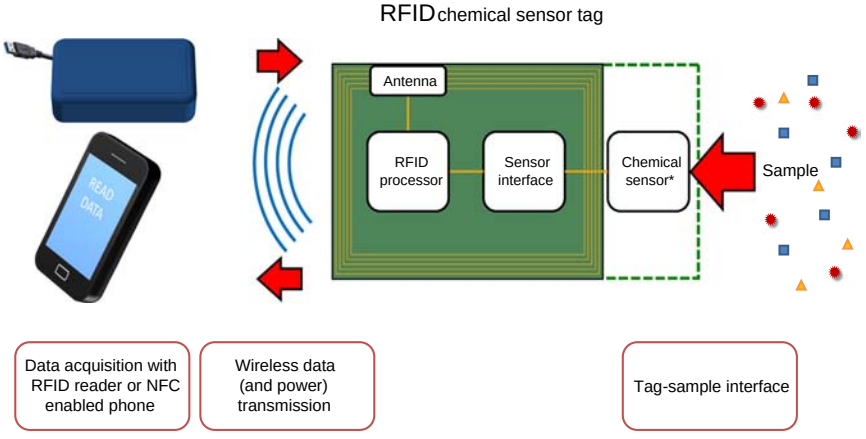

Fig. 1. General schematic of the RFID-based chemical sensor platform. *The chemical sensor can be integrated onto the tag, or may be off the tag. In this work, the optical sensing elements are off tag.

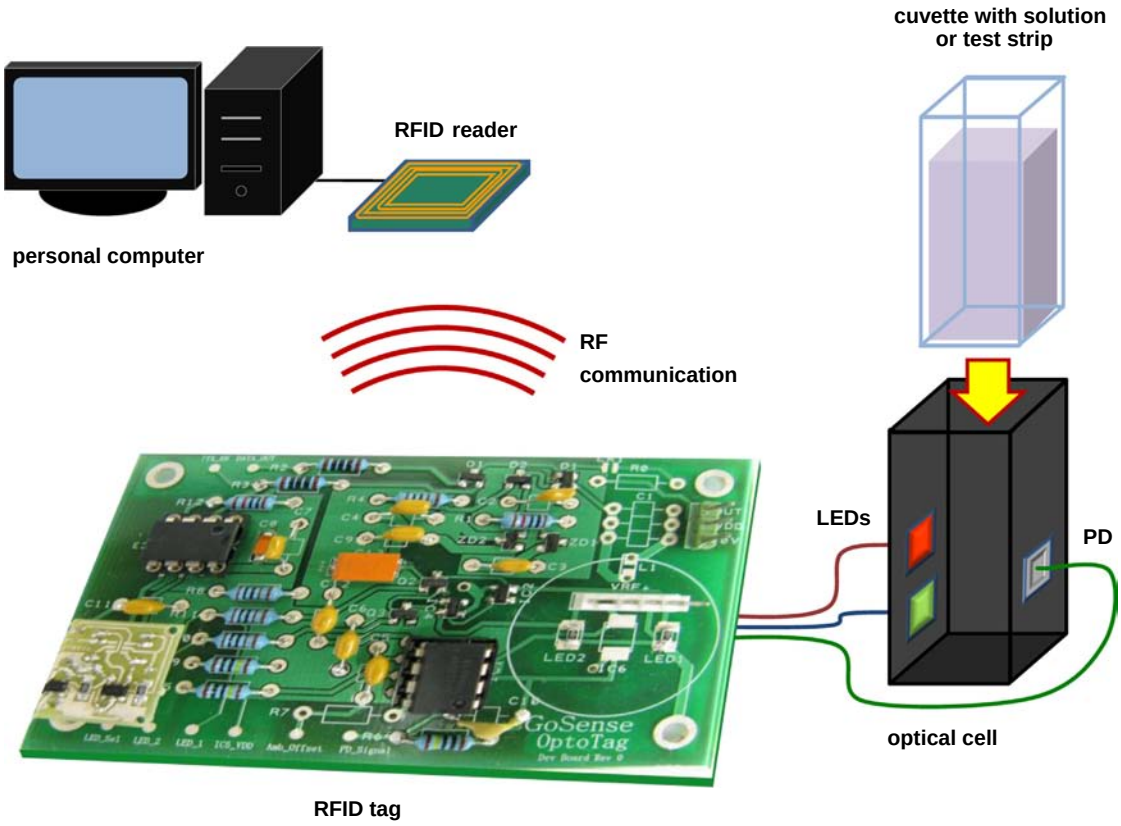

Fig. 2. Schematic illustration of the wireless photometer in the experimental setup. Objects in the figure are not to scale.

(RAK Printed Circuits Ltd., Saffron Walden, UK). The microcontroller is interfaced to the optoelectronic components (LEDs and photodiode) to allow full programmable control of the photometer interface via the embedded software.

2.1.2. Optical cell configuration

The optical cell detection system consists of red and green surface mount LEDs (HSMx-C150, Avago Technologies Ltd., San Jose, CA, USA) assembled facing a surface mount photodiode (BPW34S, Osram Opto Semiconductors GmbH, Regensburg, Germany). The LEDs were chosen based on the spectral characterisation of the dye which was performed with a laboratory UV–vis spectrophotometer (DMS 80, Varian Inc., Palo Alto, CA, USA). The optoelectronic components are positioned on opposite sides of a cell holder made from a black ABS potting box (RS Components Ltd., Corby, UK) and are interfaced to the radio-frequency tag. The cell holder is designed to accept a standard laboratory cuvette and therefore has internal dimensions of approximately 1.3 cm $\times$ 1.3 cm $\times$ 5 cm.

2.1.3. Absorption measurements with the smart tag photometer

All measurements were performed in the following way: A cuvette filled with a measuring solution was placed and closed within the cell holder of the optical cell of the photometer. The RFID tag embedded software first turns on the red LED for 5 ms and simultaneously measures the light intensity signal from the photodiode amplifier generated by the light transmitted through the optical cell. Absorbance was calculated as $A = \log(I_0/I)$ where I_0 is the photodiode amplifier signal measured without a sample (as a reference) and I is the signal measured in the sample solution. The second LED (green) was not used in this series of experiments, but is available if needed, e.g. to provide a reference signal at an isobestic wavelength as we have previously demonstrated [26]. Finally, the photometer goes into a very low-power standby mode for approximately 5 s in order to scavenge energy from the RF field before autonomously starting another measurement cycle. Independent absorption measurements were also performed with the laboratory spectrophotometer which was used as a reference system.

2.2. Methods

2.2.1. Photometry in solution

Solutions of different concentrations of lipophilised Nile Blue derivative dye, also known as ETH 5294, (10^{-6} M to 10^{-5} M, with 0.25×10^{-6} M increments) were prepared by weighing 3-octadecanoylimino-7-(diethylamino)-1,2-benzophenoxazin (Sigma–Aldrich, St. Louis, MO, USA), referred to as NB in the following text, dissolving it in ethanol (Carlo Erba Reagenti, Arese, Italy) and subsequently diluting the stock solution with ethanol to obtain the desired concentration. 0.01 M HCl solution was prepared from concentrated HCl (Carlo Erba Reagenti, Arese, Italy) and was added to each dye solution in a 1% volume fraction to ensure complete protonation of NB and absorption at 660 nm. These solutions were used for calibration of the smart tag photometer.

2.2.2. Potassium-selective optode measurements

The following chemicals were used for the preparation of potassium-sensing thin films: high-molecular-weight poly (vinyl chloride) (PVC), dibutyl sebacate (DBS), tetrahydrofuran (THF), valinomycin, NB, and Potassium tetrakis(4-chlorophenyl)borate (PTCB), all used as supplied (Sigma–Aldrich, St. Louis, MO, USA). The films were prepared according to [33], with minor modifications. Chemical cocktail mixtures were made by dissolving 67 mg of PVC, 140 mg of DBS, 4.4 mg of valinomycin, 2.3 mg of NB and 2.2 mg of PTCB in 1.5 mL of THF. The cocktails were homogenised

for 15 min in an ultrasonic bath (Transsonic T 460/H, Elma Hans Schmidbauer GmbH & Co. KG, Singen, Germany) and left overnight. Thin films were made by spin-coating 0.1 mL of the cocktail onto 2.5 cm × 2.5 cm polyester sheets using a commercial spin-coater (KW-4 A spin coater, Chemat Technology Inc., Northridge, CA, USA) at 1200 rpm for 40 s after which they were stored in the dark for at least 24 h. The films were then cut into 2.5 cm × 0.8 cm strips in order to be used in all of the following experiments.

Calibration solutions and procedures for measurements with the potassium optodes were prepared in the following way: 0.067 M phosphate buffer solution (pH 7.40) was prepared from sodium dihydrogen phosphate and disodium hydrogen phosphate (Kemika d.d., Zagreb, Croatia). 0.1 M potassium chloride (KCl) solution was prepared by weighing dry KCl (Kemika d.d., Zagreb, Croatia) and dissolving it in the buffer. A set of calibration solutions (down to 10^{-6} M) were prepared by dilution of the 0.1 M KCl stock solution with the buffer. Use of buffer was prerequisite due to the known cross-sensitivity of these potassium optodes to pH. Calibration solutions were used with the potassium-sensitive test strips to construct a calibration curve for the ion-selective optode measurements. The measurement procedure was as follows: a potassium-sensitive test strip was placed into a cuvette containing 0.01 M HCl solution and allowed to equilibrate for 10 min, after which the photodiode signal was recorded. This signal was used to calculate A_{HCl}. After this, the strip was placed in a cuvette containing a buffered KCl solution and the photodiode signal was recorded after 3 min of equilibration and used to calculate A.

3. Results

3.1. RFID sensor platform and smart tag photometer operation

The general structure of the RFID chemical sensor platform developed is shown in Fig. 1. Each tag has an ISO15693 RFID processor and antenna, together with a sensor interface. The sensor interface is configurable depending on the sensor type, and can interface to optical, amperometric, potentiometric, conductometric and resistive bridge-type sensors. The chemical sensor element (LED/photodiode, pH electrode, ion-selective electrode, thin-film conductometric electrode, enzyme electrode, etc.) can be integrated on the tag as we have previously demonstrated [26], or may be an external sensing element [30,32]. In the work reported here, the sensor element comprises a photometric cell with LED light source and silicon photodiode detector, Fig. 2. Our approach to the fusion of chemical sensors with RFID technology is based around use of a digital RFID core with configurable analogue sensor inputs. The reconfigurable analogue inputs for different types of chemical sensors allow building of autonomous (bio) chemical sensors with integrated wireless capability at low cost. Ultimately, our objective is to evolve the platform so that it is easily adapted for “plug and play” with many different types of chemical sensor.

The optoelectronic interface for the photometer smart tag is built around a standard spectrometer sample cuvette. The surface mount LED and silicon photodiode are aligned on opposite faces of the sample cuvette as shown, this configuration allowing absorption photometry measurements. The final system thus comprises the credit card sized wireless photometer, the sample cuvette with LED and photodiode, and a personal computer as shown in Fig. 2. The photometer is wirelessly linked to the personal computer through a commercial RFID reader which energises and communicates with the photometer over a range of up to 10 cm. The photometer operates in *passive mode* – it is powered by scavenging energy from the electromagnetic field generated by the RFID reader and therefore does not require a battery or power source.

3.2. Choice of model experiments

The analytical performance of the wireless photometer was subsequently evaluated through two applications of photometry, serving as proof-of-concept experiments. The first was photometry in solution where the photometer was used for determination of concentration of the derivative of Nile Blue dye (NB) in ethanol solutions.

The second application demonstrated applicability of the wireless photometer in a typical chemical sensor arrangement, using ion-selective optodes [34]. Here, the wireless photometer was used to measure the concentration of potassium ions with valinomycin based plasticized PVC optodes containing NB dye as a chromoionophore.

NB is a lipophilised derivative of a pH-sensitive dye, Nile Blue, which in its protonated form has two absorption maxima at 660 nm and 615 nm respectively (shown in immobilised form in Fig. 4, Section 3.4). Therefore, a red LED which has a peak wavelength at 660 nm was chosen as the light source for these experiments.

3.3. Wireless photometry in solution

The calibration plot for determination of NB in ethanol solutions was obtained with the wireless photometer. Five independent measurements of absorbance were conducted for each of five different concentrations of NB. Each point on the graph represents the mean value of five different measurements per concentration. A linear regression of the data returns the following calibration function: $A = 40196 \times c(\mathrm{NB})/\mathrm{M} - 0.016$ ($R^2 = 0.996$), proving good agreement with the Lambert–Beer law. Table 1 shows the precision of the measurements, expressed as the standard deviation and relative standard deviation of NB concentrations. Standard deviations and relative standard deviations obtained with the laboratory spectrophotometer are also shown for reference.

In order to validate the accuracy of the wireless photometer, the concentrations of the NB solutions were independently determined with the laboratory spectrophotometer to provide reference values. The correlation plot showing concentration of NB calculated from the calibration function of the wireless photometer plotted against concentration of NB calculated from the calibration function of the laboratory spectrophotometer for a total of 25 different solutions is shown in Fig.3. A unity-slope linear fit would be expected in the case of perfect correlation between the two measurement systems. The actual linear fit of the data has a slope of 1.003, with a very good linearity ($R^2 = 0.997$).

3.4. Test strip based wireless optical sensing

The wireless photometer was then used with optical test strips for the determination of potassium ion concentration. This is based on bulk optode membranes where the extraction of the analyte from the sample into the bulk of the membrane generates a change in the optical properties of the sensing layer. The sensing mechanism and specific behaviour of potassium ion-sensitive bulk optode membranes incorporating valinomycin as an ionophore and a lipophilised pH indicator as a chromoionophore is well known [34,35]. Since the response of the optode is based on an ion-exchange mechanism, H^+ and K^+ between the membrane and the solution, all experiments were performed in buffers of constant pH value (pH = 7.40).

For this experiment, potassium-ion sensitive optodes were fabricated and first characterised with the laboratory spectrophotometer.

Table 1
Standard deviations and relative standard deviations of NB concentrations calculated from absorbance measurements with the wireless photometer and reference spectrophotometer.

c(NB)/M	St dev, wireless photometer ($n=5$)	RSD, %	St dev, spectrophotometer ($n=5$)	RSD, %
1.0×10^{-6}	8.0×10^{-8}	9.4	1.0×10^{-8}	0.99
2.5×10^{-6}	1.2×10^{-7}	4.6	4.6×10^{-8}	1.9
5.0×10^{-6}	1.2×10^{-7}	2.3	1.6×10^{-8}	0.32
7.5×10^{-6}	8.2×10^{-8}	1.1	4.1×10^{-8}	0.55
1.0×10^{-5}	4.8×10^{-8}	0.48	1.5×10^{-8}	0.15

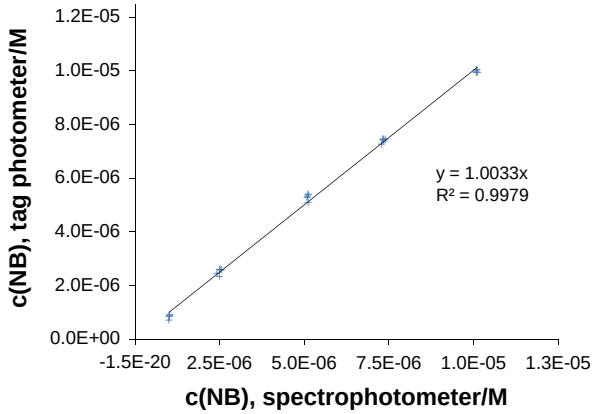

Fig. 3. Correlation plot showing NB concentration obtained with the wireless photometer plotted against concentration obtained with a laboratory spectrophotometer considered a reference procedure.

The typical spectral response of an optode to varying concentration of potassium ion is shown in Fig. 4. On exposure to potassium ion solutions, the optode film changes colour from blue (absorption maxima at 615 nm and 660 nm) to purple (absorption maximum at 540 nm). The absorbance measured at 660 nm can be related to the concentration of potassium ion in solution, and it has previously been shown that the ratio between absorbance of the thin film in potassium ion solution and absorbance in a 0.01 M HCl reference solution A/A_{HCl} can serve as an analytical parameter for obtaining a calibration curve [36].

The response time, expressed as the time it takes for the sensor to reach 95% of its response upon immersion of the fully protonated test strips in a 10^{-4} M KCl (pH 7.40) in phosphate buffer solution, was determined to be 104 s. The dynamic response is shown in Fig. 4 (inset).

The calibration curve for this system obtained with the wireless photometer is shown in Fig. 5. The relationship between the analytical parameter, A/A_{HCl}, and the logarithm of potassium concentration is sigmoidal, so data points were fitted to a Boltzmann function. The curve shows excellent adjustment ($R^2=0.99956$).

Fig. 6 shows the correlation plot for K^+ concentration determined with the wireless photometer against K^+ concentration determined with the laboratory spectrophotometer. K^+ concentrations were calculated from absorbance data using each instruments' respective Boltzmann calibration function. The linear fit of the correlated concentrations is $y=0.971x-0.135$ ($R^2=0.977$).

4. Discussion

Overall, good correlation between the performance of the wireless photometer and the reference laboratory UV–vis spectrophotometer

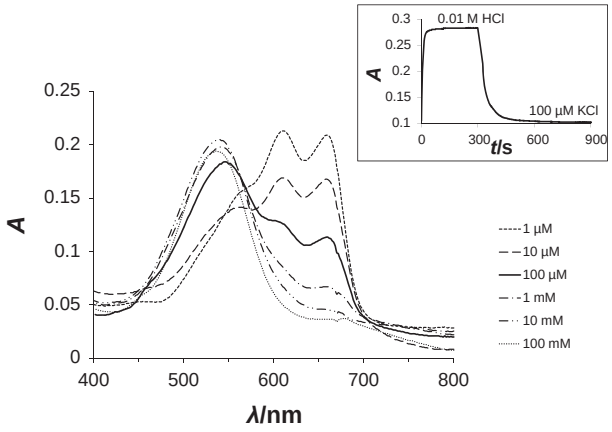

Fig. 4. Absorption spectra of potassium-sensing thin films in different concentrations of KCl recorded with a laboratory spectrophotometer. KCl concentrations range from 10^{-6} M to 10^{-1} M. The inset shows absorbance at 660 nm over time, upon immersion of a fully protonated test strip into a 10^{-4} M KCl (pH 7.40) in phosphate buffer solution.

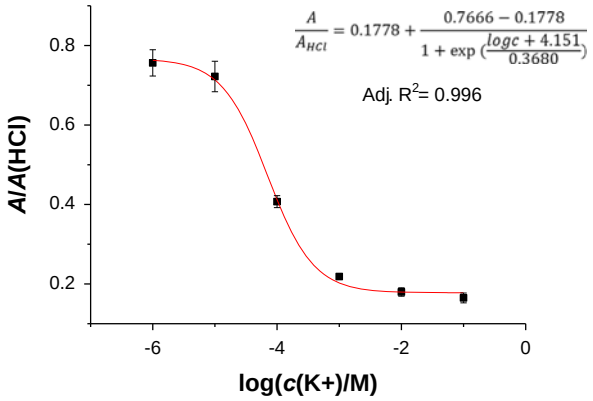

Fig. 5. Response of potassium-sensing thin films to different KCl concentrations recorded with the wireless photometer. Boltzmann function fit can be used as calibration function. Error bars represent standard deviation of the results.

was observed, both for photometry in solutions as well as with potassium-ion sensing thin films. When measuring in solutions, the photometer showed excellent linearity over the concentration range tested (1.0×10^{-6} to 1.0×10^{-5} of NB), showing good agreement with the Lambert–Beer law. Precision of the wireless photometer, expressed as standard deviation of NB concentration, was less than 1.2×10^{-7} M compared to less than 4.6×10^{-8} M obtained with the reference laboratory spectrophotometer. These are very acceptable results considering the relative size, weight, portability and cost of the two instruments. Potassium-sensitive thin films have been used here as a proof-of-principle model optode system, but clearly optical absorbance or reflectance measurements could be performed with various other colourimetric assays in solution or immobilised form. This approach is especially attractive for the quantitative analysis of ultra low-cost optical point-of-care diagnostic tests. Examples of which include paper-based microfluidic devices as recently critically reviewed by Yetisen et al. [37]. Other recent examples of low-cost mobile analytical systems include the optical determination of protein and glucose in urine using camera phones [38], and a hand-held optical colorimeter for measuring transmittance through paper for quantifying the concentration of analytes in biological fluids [39]. Rearrangement of the optical components of the wireless smart tag into a planar configuration allows the photometer to work in a reflectance mode [40].

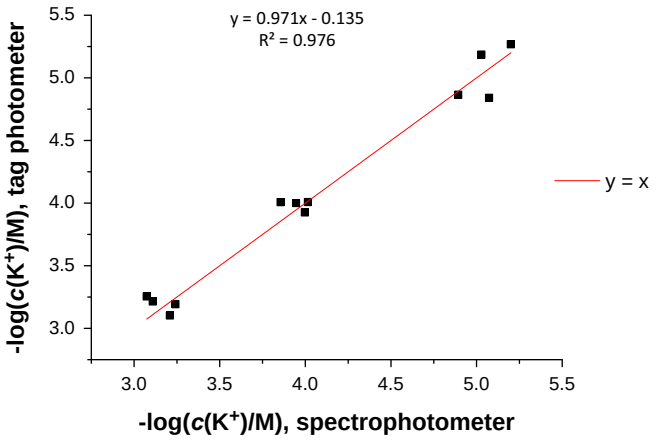

Fig. 6. Correlation plot for K^+ concentration determined with the wireless photometer against K^+ concentration determined with the laboratory spectrophotometer. A unity slope straight line is shown for reference.

The wireless smart tag photometer may also be compatible with a number of new and emerging sensor application areas, especially wearable and textile-based optical chemical sensors (e.g. for sweat analysis in physiological and sports fitness monitoring) [41–43], smart food packaging [44,45] and smart laboratory containers [46]. An interesting example of this type of system is a wearable monitoring system realised using low-cost light-emitting diodes (LEDs) and an autonomous wearable micro-fluidic platform to monitor pH of sweat [47]. Another potential application area for the smart tag is optical sensing in disposable microfluidic and lab-on-a-chip systems [48]. Further miniaturisation of the photometer could, for example, allow its functional integration into wirelessly powered microfluidic lab-on-a-chip systems [49].

These results have proven the feasibility of the wireless photometer and justify its further development, which is currently underway in our laboratory. The main short-coming of the present system encountered during the course of this work is the input power requirement of the LED light source. We endeavour to minimise this through the use of low-power LEDs and by implementing a constant current pulse-width modulated drive strategy. Still, the LED requires a relatively large amount of power (relative to the rest of the tag) which impacts on the wireless power/read range of the tag, reducing the reliable read range from 50 cm to about 10 cm when energised with the RFID reader. A new mobile photometer, based on the next generation RFID tag, is being developed that will have several improvements over the one presented here. The new photometer tag will be compatible with the near field communication (NFCv) standard as well as RFID. NFC is a wireless communication technology which is currently being implemented in a large number of Smartphones [50]. This means that with appropriate application software, a Smartphone could be used to collect data from the wireless photometer, thereby eliminating the need for a conventional RFID reader or computer – making it a truly mobile analytical platform. The new photometer will also include an on-board battery to assist in powering the LED light source, and 1 Mbit data memory. These improvements will enable autonomous measurement and data logging (up to 64,000 samples) of chemical absorption data without the need for a nearby RFID reader and without the need for operator intervention.

5. Conclusion

This paper presents a novel miniaturised and portable, low-cost, low-power wireless photometer designed around the passive RFID smart tag format. The analytical performance of the wireless photometer has been demonstrated via a set of optical absorption-based analytical experiments, with excellent data agreement with a reference laboratory instrument. The photometer operates without a battery or power source since it scavenges energy from the RF electromagnetic field of the RFID reader. The photometer has potential application in photometric systems where a change in colour intensity is to be measured. By changing the optoelectronic components of the optical cell to match the desired sensing chemistry, a diverse range of colour-change sensor chemistries could be implemented. With a wide variety of potential analytes, and the ability to modify the specific chemistry and optical measurement strategy, numerous mobile, wearable and *vanguard* applications for this type of sensor can be envisaged – from fresh water quality monitoring, to real-time sweat analysis. With the advent of the Internet of Things on the horizon, devices such as this photometer, that combine low-cost chemical sensing with wireless communications, will provide analytical platforms for enhanced ambient intelligence. The smart tag presented in this work is fully compatible with such application predictions.

Acknowledgements

This work was co-financed by The National Foundation for Science, Higher Education and Technological Development of the Republic of Croatia (NZZ) through the project *Distributed wireless sensors for smart chemical and biological detection systems: chemo- and biosensor interface and applications development*, with additional support from the Ministry of Science, Education and Sport of the Republic of Croatia (MSES) under science project grant number 125-0000000-3221, both of which are gratefully acknowledged.

References

[1] R.A. Potyrailo, C. Surman, N. Nagraj, A. Burns, Chem. Rev. 111 (2011) 7315–7354.
[2] R. Byrne, D. Diamond, Nat. Mater. 5 (2006) 421–424.
[3] D. Diamond, K.T. Lau, S. Brady, J. Cleary, Talanta 75 (2008) 606–612.
[4] L. Ruiz-Garcia, L. Lunadei, P. Barreiro, J.I. Robla, Sensors 9 (2009) 4728–4750.
[5] J.F. van Staden, R.I. Stefan-van Staden, S.C. Balasoiu, Crit. Rev. Anal. Chem. 40 (2010) 226–233.
[6] R.A. Potyrailo, N. Nagraj, C. Surman, H. Boudries, H. Lai, J.M. Slocik, N. Kelley-Loughnane, R.R. Naik, TrAC Trends Anal. Chem. 40 (2012) 133–145.
[7] L. Atzori, A. Iera, G. Morabito, Comput. Netw. 54 (2010) 2787–2805.
[8] E. Abad, S. Zampolli, S. Marco, A. Scorzoni, B. Mazzolai, A. Juarros, D. Gomez, I. Elmi, G.C. Cardinali, J.M. Gomez, F. Palacio, M. Cicioni, A. Mondini, T. Becker, I. Sayhan, Sens. Actuators B-Chem. 127 (2007) 2–7.
[9] U. Altenberend, F. Molina-Lopez, A. Oprea, D. Briand, N. Bârsan, N.F. De Rooij, U. Weimar, Sens. Actuators B-Chem, 187, 2013, 280–287.
[10] D. Briand, A. Oprea, J. Courbat, N. Bârsan, Mater. Today 14 (2011) 416–423.
[11] A. Pletersek, M. Sok, J. Trontelj, J. Med. Syst. 36 (2012) 3733–3739.
[12] R.A. Potyrallo, W.G. Morris, Anal. Chem. 79 (2007) 45–51.
[13] R.A. Potyrailo, N. Nagraj, Z.X. Tang, F.J. Mondello, C. Surman, W. Morris, J. Agric. Food Chem. 60 (2012) 8535–8543.
[14] O.S. Wolfbeis, Fiber Optic Chemical Sensors and Biosensors, CRC Press, Inc., Boca Raton, 1991.
[15] D. Betteridge, E.L. Dagless, B. Fields, N.F. Graves, Analyst 103 (1978) 897–908.
[16] P.K. Dasgupta, I.-Y. Eom, K.J. Morris, J. Li, Anal. Chim. Acta 500 (2003) 337–364.
[17] M. O'Toole, D. Diamond, Sensors 8 (2008) 2453–2479.
[18] L.F. Capitán-Vallvey, A.J. Palma, Anal. Chim. Acta 696 (2011) 27–46.
[19] M. Pokrzywnicka, L. Tymecki, R. Koncki, Talanta 96 (2012) 121–126.
[20] L. Rovati, F. Docchio, Meas. Sci. Technol. 11 (2000) 185–192.
[21] M.H. Sorouraddin, A. Rostami, M. Saadati, Food Chem. 127 (2011) 308–313.
[22] D. Orpen, S. Beirne, C. Fay, K.T. Lau, B. Corcoran, D. Diamond, Sens. Actuators B-Chem. 153 (2011) 182–187.
[23] D.J. Cocovi-Solberg, M. Miró, V. Cerdà, M. Pokrzywnicka, Ł. Tymecki, R. Koncki, Talanta 96 (2012) 113–120.
[24] R. Shepherd, S. Beirne, K.T. Lau, B. Corcoran, D. Diamond, Sens. Actuators B-Chem. 121 (2007) 142–149.
[25] C. Fay, K.-T. Lau, S. Beirne, C. Ó Conaire, K. McGuinness, B. Corcoran, N.E. O'Connor, D. Diamond, S. McGovern, G. Coleman, R. Shepherd, G. Alici, G. Spinks, G. Wallace, Sens. Actuators B-Chem. 150 (2010) 425–435.
[26] I.M. Steinberg, M.D. Steinberg, Sens. Actuators B-Chem. 138 (2009) 120–125.
[27] Y. Yazawa, T. Oonishi, K. Watanabe, R. Nemoto, A. Shiratori, Jpn J. Appl. Phys. 49 (2010) 04DL13.

[28] M.D. Steinberg, I. Zura, I.M. Steinberg, in: Presented at Biosensors 2008, Shanghai, May 14–16, 2008.
[29] M.D. Steinberg, I. Steinberg, Contactless microenvironment sensor, Patent, GB0908363.5, 2010.
[30] P. Kassal, I.M. Steinberg, M.D. Steinberg, Sens. Actuators B-Chem. 184 (2013) 254–259.
[31] M. Valcarcel, S. Cardenas, Trac-Trends Anal. Chem. 24 (2005) 67–74.
[32] M. Novell, T. Guinovart, I.M. Steinberg, M. Steinberg, F.X. Rius, F.J. Andrade, Analyst 138 (2013) 5250–5257.
[33] E. Malavolti, A. Cagnini, G. Caputo, L. Della Ciana, M. Mascini, Anal. Chim. Acta 401 (1999) 129–136.
[34] K. Seiler, W. Simon, Anal. Chim. Acta 266 (1992) 73–87.
[35] E. Bakker, P. Bühlmann, E. Pretsch, Chemical Reviews 97 (1997) 3083–3132.
[36] A. Palma, A. Lapresta-Fernández, J. Ortigosa-Moreno, M. Fernández-Ramos, M. Carvajal, L. Capitán-Vallvey, Anal. Bioanal. Chem. 386 (2006) 1215–1224.
[37] A.K. Yetisen, M.S. Akram, C.R. Lowe, Lab on a Chip 13 (2013) 2210–2251.
[38] A.W. Martinez, S.T. Phillips, E. Carrilho, S.W. Thomas, H. Sindi, G.M. Whitesides, Analytical Chemistry 80 (2008) 3699–3707.
[39] A.K. Ellerbee, S.T. Phillips, A.C. Siegel, K.A. Mirica, A.W. Martinez, P. Striehl, N. Jain, M. Prentiss, G.M. Whitesides, Anal. Chem. 81 (2009) 8447–8452.
[40] I.M. Steinberg, M.D. Steinberg, Sens. Actuators B-Chem. 138 (2009) 120–125.
[41] L. Van der Schueren, K.De Clerck, Color. Technol. 128 (2012) 82–90.
[42] S. Coyle, K.T. Lau, N. Moyna, D. O'Gorman, D. Diamond, F. Di Francesco, D. Costanzo, P. Salvo, M.G. Trivella, D.E. De Rossi, N. Taccini, R. Paradiso, J.A. Porchet, A. Ridolfi, J. Luprano, C. Chuzel, T. Lanier, F. Revol-Cavalier, S. Schoumacker, V. Mourier, I. Chartier, R. Convert, H. De-Moncuit, C. Bini, IEEE T. Inf. Technol. Biomed. 14 (2010) 364–370.
[43] M. Caldara, C. Colleoni, E. Guido, V. Re, G. Rosace, Sens. Actuator B-Chem. 171 (2012) 1013–1021.
[44] C. von Bultzingslowen, A.K. McEvoy, C. McDonagh, B.D. MacCraith, I. Klimant, C. Krause, O.S. Wolfbeis, Analyst 127 (2002) 1478–1483.
[45] A. Pacquit, J. Frisby, D. Diamond, K.T. Lau, A. Farrell, B. Quilty, Food Chem. 102 (2007) 466–470.
[46] M.B. Mikkelsen, R. Marie, J.H. Hansen, D. Wencel, C. McDonagh, H.O. Nielsen, A. Kristensen, J. Micromech. Microeng. 21 (2011) 115008.
[47] V.F. Curto, S. Coyle, R. Byrne, N. Angelov, D. Diamond, F. Benito-Lopez, Sens. Actuator B-Chem. 175 (2012) 263–270.
[48] B. Kuswandi, Nuriman, J. Huskens, W. Verboom, Anal. Chim. Acta 601 (2007) 141–155.
[49] W. Qiao, G. Cho, Y.H. Lo, Lab Chip 11 (2011) 1074–1080.
[50] E. Strömmer, M. Hillukkala, A. Ylisaukko-oja, Ultra-low power sensors with near field communication for mobile applications, in: L. Orozco-Barbosa, T. Olivares, R. Casado, A. Bermúdez (Eds.), Wireless Sensor and Actor Networks, Springer, US, 2007, pp. 131–142.